SCIENTIFIC REPORTS

OPEN

A new insight into the immobilization mechanism of Zn on biochar: the role of anions dissolved from ash

Received: 12 April 2016
Accepted: 01 September 2016
Published: 19 September 2016

Tingting Qian[1], Yujun Wang[1], Tingting Fan[1,2], Guodong Fang[1] & Dongmei Zhou[1]

Biochar is considered to be a promising material for heavy metal immobilization in soil. However, the immobilization mechanisms of Zn^{2+} on biochars derived from many common waste biomasses are not completely understood. Herein, biochars (denoted as PN350, PN550, WS350, and WS550) derived from pine needle (PN) and wheat straw (WS) were prepared at two pyrolysis temperatures (350 °C and 550 °C). The immobilization behaviors and mechanisms of Zn^{2+} on these biochars were systematically investigated. The results show that compared with biochars produced at low temperature, biochars produced at high temperature contained higher amounts of ash and exhibited much higher sorption capacities of Zn^{2+}. By using Zn K-edge EXAFS spectroscopy, we find that the formation of various Zn precipitates/minerals, which was caused by the release of OH^-, CO_3^{2-}, and Si species from biochar, was the immobilization mechanism of Zn^{2+} on PN and WS biochars. Hydrozincite and $Zn(OH)_2$ were the main species formed on PN350, PN550, and WS350; while on WS550, besides hydrozincite, a large fraction of hemimorphite was formed. The occurrence of hydrozincite and hemimorphite on biochar during Zn^{2+} immobilization is firstly reported in our study, which provides a new insight into the immobilization mechanism of Zn^{2+} on biochar.

Zinc (Zn) is an essential nutrient for living organisms[1], however, an excess supply of Zn can lead to toxic effect on plants[2–4] and microorganisms[5,6] in soil. Due to anthropogenic activities (such as industrial activities, sludge application, waste water irrigation, etc.[3]), Zn can be easily released into soil environment[7], which could pose a threat to the health of ecosystems[8] and even to human beings[9,10]. As free Zn ions are the main species for Zn toxicity[1,5], the immobilization of free Zn ions by some materials would reduce its bioavailability and toxicity in soil. Thus, materials which are effective in Zn immobilization should be developed.

As an emerging carbonaceous material, biochar has been extensively studied especially in the field of soil remediation[11–17]. The carbonaceous residue and entrained minerals (ash) are two main components of biochar[18], they perform different functions in soil remediation. The carbonaceous residue can adsorb and retain water[19] and some organic pollutants[20–23]; the ash can provide nutrient elements and improve soil pH[24]. In terms of heavy metal immobilization, both of the two components could be involved in the process. Plenty of studies have reported the immobilization behavior of Zn on biochars derived from different biomass (such as hardwood[25,26], corn straw[25], sugarcane straw[27], dairy manure[28], and meat and bonemeal[29]), and some of them have proposed the immobilization mechanisms which implied more important role of ash on biochar on Zn immobilization[27,28,30]. Xu *et al.* studied the sorption behavior of Zn on biochar derived from dairy manure, and found that large amounts of PO_4^{3-} and CO_3^{2-} were released from biochar and reacted with Zn^{2+} to form Zn phosphate and Zn carbonate[28]. With the help of P K-edge XANES spectroscopy, Wegner *et al.* found that hopeite ($Zn_3(PO_4)\cdot 2H_2O$) or a similar Zn-P phase were formed, when biochar was used to immobilize Zn in the sewage field soils[30]. In addition to forming Zn precipitates, the formation of Zn complexes on biochar surface also led to Zn immobilization[29]. By using the method of extended X-ray absorption fine structure (EXAFS) spectroscopy, Betts *et al.*[29] found that Zn bound to phosphate groups in meat and bonemeal biochar in a monodentate inner-sphere surface complex.

[1]Key Laboratory of Soil Environment and Pollution Remediation, Institute of Soil Science, Chinese Academy of Sciences, Nanjing 210008, China. [2]University of Chinese Academy of Sciences, Beijing 100049, China. Correspondence and requests for materials should be addressed to D.Z. (email: dmzhou@issas.ac.cn)

Biochar	K	Ca	Mg	Al	Fe	Zn	P	pH and pH_{PZC}*
PN350	9.8 ± 0.6	15.7 ± 0.3	3.0 ± 0.2	1.4 ± 0.0	0.9 ± 0.0	0.076 ± 0.001	1.8 ± 0.0	7.9 ± 0.1
PN550	13.6 ± 0.0	23.7 ± 0.7	4.6 ± 0.2	2.1 ± 0.0	1.3 ± 0.0	0.106 ± 0.003	2.7 ± 0.0	9.6 ± 0.0
WS350	31.8 ± 0.4	9.7 ± 0.2	2.6 ± 0.0	1.8 ± 0.0	1.7 ± 0.0	0.061 ± 0.009	1.3 ± 0.0	8.2 ± 0.0
WS550	38.8 ± 0.6	12.3 ± 0.7	3.8 ± 0.1	2.3 ± 0.1	2.2 ± 0.0	0.060 ± 0.001	1.7 ± 0.0	9.7 ± 0.0
$PN350_D$	0.29 ± 0.02	5.0 ± 0.5	1.8 ± 0.0	0.46 ± 0.00	0.25 ± 0.01	0.056 ± 0.002	0.12 ± 0.00	4.3 ± 0.1
$PN550_D$	0.24 ± 0.01	4.7 ± 0.1	4.0 ± 0.1	0.91 ± 0.02	0.28 ± 0.00	0.083 ± 0.003	1.20 ± 0.02	5.4 ± 0.1
$WS350_D$	0.02 ± 0.00	1.0 ± 0.1	0.7 ± 0.0	0.13 ± 0.05	0.21 ± 0.01	0.016 ± 0.003	0.05 ± 0.00	4.4 ± 0.0
$WS550_D$	0.06 ± 0.00	3.3 ± 0.1	2.2 ± 0.0	0.12 ± 0.01	0.31 ± 0.01	0.029 ± 0.002	0.22 ± 0.00	5.5 ± 0.1

Table 1. The contents of some common elements (mg g^{-1}), and the pH and pH_{PZC} of biochars. *The dissolution of the ash in raw biochar could consume a large amount of H^+, which makes the pH_{PZC} data of raw biochars unreliable, thus only the pH_{PZC} of de-ashed biochars has been tested.

Feedstock types and pyrolysis temperature are two main factors influencing biochar property[18]. As a wide variety of biomasses can be used for biochar production, previous studies on Zn^{2+} immobilization behavior of limited type of biochars are far from enough. To explore the immobilization mechanisms of Zn^{2+} on different biochars and provide more basic data for biochar application, studies which are focused on biochars produced by other waste biomasses need to be done. Although many studies have mentioned the effect of pyrolysis temperature on biochar property[20,31–34], few studies systematically investigated the effect of pyrolysis temperature on immobilization behavior of Zn^{2+} on biochar and elucidated the internal connection between pyrolysis temperature, biochar property, and immobilization behavior of Zn^{2+} on biochar. In this study, biochars produced by pine needle (PN) and wheat straw (WS) were chosen for investigation, to our knowledge, there is no published work concentrated on Zn^{2+} immobilization behavior of biochars derived from these biomasses. Two temperatures were chosen for biochar preparation, and the Zn^{2+} immobilization behaviors of biochars produced by different temperature were compared through several sorption experiments (i.e. sorption kinetics, sorption isotherms, and the effect of pH). To reveal the importance of the ash on biochars on Zn immobilization, the ash was removed from biochars, and the Zn^{2+} immobilization behaviors of de-ashed biochars were compared with those of the raw biochars. To explore the immobilization mechanisms, the methods of Zn K-edge EXAFS spectroscopy and X-ray Powder Diffraction (XRD) were used for biochar characterization. Through this study, the Zn species immobilized by PN and WS biochars will be identified, the immobilization mechanisms and the relation between pyrolysis temperature and immobilization behaviors of Zn^{2+} on studied biochars will be clear.

Results and Discussion

Characterization of PN and WS biochars. The contents of the common elements (i.e. K, Ca, Mg, Al, Fe, Zn, and P) in biochars were determined and listed in Table 1. The contents of most studied elements in biochars produced at 550 °C were higher than those in biochars produced at 350 °C, which suggested that the ash contents of biochars produced at 550 °C were higher than those of biochars produced at 350 °C. The high Ca contents in PN biochars and high K contents in WS biochars implied that, in addition to immobilizing heavy metal, PN and WS biochars could also supply large amounts of nutrient elements to the soil. When raw biochars were washed by HCl/HF solution, the contents of the elements substantially dropped, this means that the factor of ash which may influence the sorption of Zn can be excluded in de-ashed biochars. The pHs of raw biochars and the pH_{PZC} of de-ashed biochars were also listed in Table 1.

To characterize the functional groups on different biochars, FTIR and XPS analysis were conducted on these biochars. The results were shown in Supplementary Fig. S1 and Supplementary Fig. S2 and Table S1.

Sorption kinetics and isotherms and the effect of initial pH on sorption behavior of Zn^{2+} on biochars. To study the sorption behaviors of Zn^{2+} on different biochars, a series of sorption experiments were conducted. Figure 1 shows the kinetics and isotherms of Zn^{2+} sorption on different biochars. From Fig. 1a we find that sorption reactions between Zn^{2+} and most biochars can reach equilibrium at 48 h, the sorption capacities of Zn^{2+} on biochars produced at 550 °C were higher than those of Zn^{2+} on biochars produced at 350 °C. Figure 1c shows that the maximum sorption capacities of Zn^{2+} on raw biochars decreased in the following order: PN550 (25.9 mg g^{-1}) > WS550 (20.4 mg g^{-1}) > WS350 (16.0 mg g^{-1}) > PN350 (3.0 mg g^{-1}). It seems that biochars with higher ash contents were more effective on Zn immobilization. From Fig. 1c,d we find that, the maximum sorption capacities of Zn^{2+} on de-ashed biochars were lower than those of Zn^{2+} on their corresponding raw biochars. Especially for biochars produced at 550 °C, the maximum sorption capacities of Zn^{2+} on biochars decreased by more than 80% when the ash was removed. These results suggested the important role of ash on Zn immobilization by biochar. Among de-ashed biochars, $WS350_D$ had the highest sorption capacity (9.4 mg g^{-1}), which may be due to the more oxygen-containing functional groups $WS350_D$ had compared with other biochars. Kinetics experiments show that sorption reactions between Zn^{2+} and most biochars can reach equilibrium at 48 h, thus the equilibrium time for the following experiments was set to be 48 h. As PN550, WS350, and WS550 had considerable sorption capacities of Zn^{2+}, several kinetics models (pseudo-first and pseudo-second-order models[35], Elovich model[36,37], and intraparticle diffusion model[38,39]) and isotherms models (Langmuir, Frendlich, and Langmuir-Frendlich models[40]) were performed on kinetics and isotherms data of these biochars, the fitting results were shown in Supplementary Tables S2 and S3.

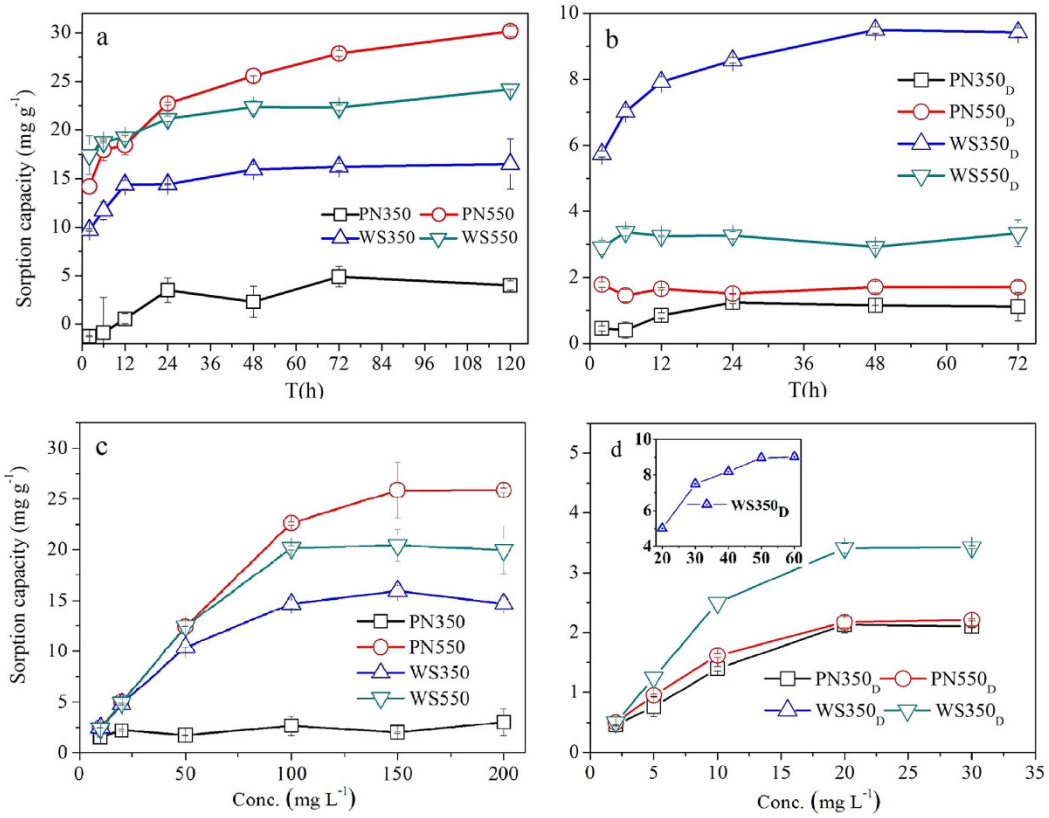

Figure 1. Kinetics and isotherms of Zn^{2+} sorption on different biochars. (**a**) Kinetics of Zn^{2+} sorption on raw biochars (the initial concentration of Zn was 150 mg L^{-1}; the solution pHs were ranged from 6.5 to 7.5 (see Fig. S3) without adjustment; (**b**) kinetics of Zn^{2+} sorption on de-ashed biochars (the initial concentration of Zn was 50 mg L^{-1}; the solution pHs were controlled to 7.0); (**c**) isotherms of Zn^{2+} sorption on raw biochars (the solution pHs were not adjusted); (**d**) isotherms of Zn^{2+} sorption on de-ashed biochars (the solution pHs were controlled to 7.0). Error bars represent ± SE (SE is the standard error of estimate). The experiments were conducted in duplicate (n = 2).

The effect of initial pH on sorption capacities of Zn^{2+} on biochars were shown in Supplementary Fig. S4. As can be seen from Fig. S4, the sorption capacities of PN550, WS350, and WS550 decreased gradually with the decrease of initial pH. Unlike the sorption behaviors of raw biochars, sharp decreases occurred on the sorption capacities of de-ashed biochars, when the initial pH decreased from 9 to 7. This may be caused by the absence of buffer effect of ash. The low sorption capacity of Zn^{2+} on PN350 under the whole pH range could be due to the low ash content.

XRD analysis. The sorption experiments showed that some Zn precipitates/minerals may be formed on biochar, thus XRD analysis were performed on these biochars. As PN350 had a relatively low sorption capacity of Zn^{2+}, we just focused on other three biochars (PN550, WS350, and WS550) and biochars loaded with Zn (denoted as PN550 + Zn, WS350 + Zn, and WS550 + Zn). Figure 2 shows the XRD spectra of the samples. The main mineral in PN550 was $CaCO_3$, the peaks of quartz in PN550 were not obvious. The peak intensities of $CaCO_3$ and quartz show that there could be large amount of CO_3^{2-} and low amount of Si contained in PN550. In WS350 and WS550, two minerals can be detected, they were quartz and sylvine. Compared with PN550, WS350 and WS550 contained larger amount of Si species.

Compared with the spectra of PN550, two more peaks appeared in the spectra of PN550 + Zn, which may belong to hydrozincite. Thus the formation of hydrozincite could be one of the mechanisms for Zn immobilization on PN550. In WS350 + Zn and WS550 + Zn, as sylvine is soluble, only quartz was maintained on WS350 and WS550. Although WS350 and WS550 had considerable sorption capacities of Zn^{2+}, none of the Zn species could be detected from the two samples by XRD analysis. This may be caused by the poor crystallinity of Zn species formed on WS350 and WS550. As the characterization way of XRD has the requirement on sample crystallinity, the method of XAFS was applied in Zn species identification.

EXAFS analysis. The k^3-weighted $\chi(k)$ functions of raw biochars and de-ashed biochars are shown in Fig. 3. To obtain the types and fractions of Zn species on these biochars, Principal Component Analysis (PCA) accompanied with Target Transformation (TT) and Linear Combination Fitting (LCF) were performed on $\chi(k)$ k^3-spectra ranging from 3–11 $Å^{-1}$ for all the samples. PCA was used to determine the number of primary

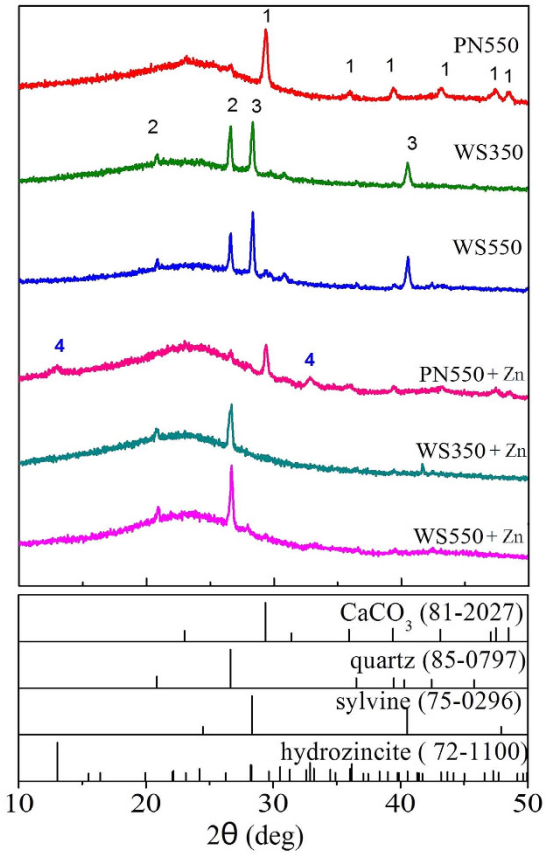

Figure 2. The XRD spectra of raw biochars and biochars loaded with Zn^{2+}. (The species are 1. $CaCO_3$ (81–2027), 2. quartz (SiO_2, 85–0797), 3. sylvine (KCl, 75–0296), 4. hydrozincite ($Zn_5(CO_3)_2(OH)_6$, 72–1100)).

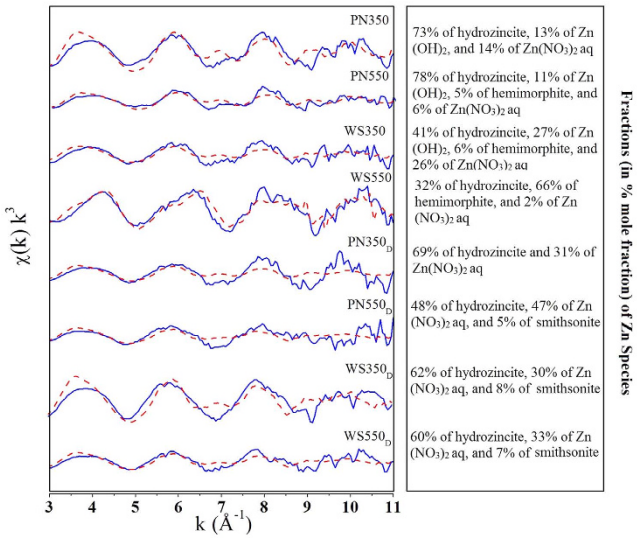

Figure 3. $\chi(k)\,k^3$-spectra of the Zn species on different biochars (solid line) and fractions of Zn species (in % mole fraction) determined by linear combination fitting. Deshed line represents the fitted line.

components which may be present in the spectra of biochars; TT was used to evaluate which species may be contained in these biochars; and LCF was applied to quantitatively analyze the Zn species on biochars. (The details on PCA, TT and LCF were shown in S1 in SI).

The result of PCA shows that five principal components may be present in the spectra of biochars. After TT by using the $\chi(k)\,k^3$-spectra of a series of standard Zn compounds (Supplementary Fig. S5), we found six Zn species (i.e. $Zn(NO_3)_2$ aqueous ($Zn(NO_3)_2$ aq), $Zn(OH)_2$, willemite (Zn_2SiO_4), smithsonite ($ZnCO_3$), hemimorphite

Biochars	pH*		CO_3^{2-}		Si species		PO_4^{3-}		Ca^{2+}		Mg^{2+}	
	B	B + Zn	B	B + Zn	B	B + Zn	B	B + Zn	B	B + Zn	B	B + Zn
PN350	8.3 ± 0.1	6.7 ± 0.1	ND	ND	0.01 ± 0.00	0.001 ± 0.000	0.03 ± 0.00	ND	0.08 ± 0.00	0.8 ± 0.2	0.07 ± 0.00	0.05 ± 0.00
PN550	10.0 ± 0.0	7.0 ± 0.1	0.3 ± 0.3	ND	0.05 ± 0.00	0.02 ± 0.00	0.04 ± 0.00	ND	0.10 ± 0.01	1.4 ± 0.0	0.06 ± 0.00	0.09 ± 0.00
WS350	9.5 ± 0.0	7.1 ± 0.0	ND	ND	0.89 ± 0.02	0.09 ± 0.00	0.06 ± 0.00	ND	0.08 ± 0.00	0.5 ± 0.1	0.09 ± 0.00	0.18 ± 0.02
WS550	10.4 ± 0.0	7.2 ± 0.1	1.1 ± 0.0	ND	1.95 ± 0.05	0.23 ± 0.00	0.06 ± 0.00	ND	0.11 ± 0.00	0.5 ± 0.1	0.08 ± 0.00	0.17 ± 0.02

Table 2. pH and Concentrations of Species (mmol L^{-1}) Involved in Zn Immobilization in the Samples.
*As some ions released from biochar may consume released OH^- in biochar + water mixture as reaction time increases, the pHs of B and B + Zn were determined at the reaction time of 2 h.

($Zn_4(H_2O)(Si_2O_7)(OH)_2$), and hydrozincite ($Zn_5(CO_3)_2(OH)_6$)) may be contained in these biochars. The number of Zn species obtained by TT was higher than that obtained by PCA, this is due to the similarity between the spectra of some standard species[41–43]. The PCA results suggested that the Zn precipitates/minerals could take up a large fraction of Zn species in biochar.

The LCF was subsequently performed on the samples using the Zn species selected by TT. The main components and their fractions in the samples were obtained and shown in Fig. 3 and Supplementary Table S6. From the fitting results (Fig. 3), we find that Zn precipitates/minerals (i.e. hydrozincite, $Zn(OH)_2$, and hemimorphite) accounted for a large share of Zn species (>70%) in raw biochars, which indicated the indispensable role of ash in biochar on Zn immobilization. High proportions of hydrozincite (>40%) and $Zn(OH)_2$ (>10%) were observed in most of the raw biochars. This result indicated that CO_3^{2-} and OH^- were two common ions for Zn immobilization. It is noteworthy that, unlike other raw biochars, WS550 contained large fraction of hemimorphite (66%). This was probably caused by the large amount of dissolved Si species released from WS550, which implied the crucial role of dissolved Si species in Zn immobilization. The species $Zn(NO_3)_2$ aq represents the Zn adsorbed on oxygen-containing functional groups (i.e. carboxyl and hydroxyl) on biochar. In PN350 and WS350, the fractions of $Zn(NO_3)_2$ aq were respectively 14% and 26%; while in PN550 and WS550, the two values dropped to 6% and 2%. These changes were due to the increase in ash contents and loss of oxygen-containing functional groups in biochars with pyrolysis temperature. In de-ashed biochars, only two main Zn species, hydrozincite and $Zn(NO_3)_2$ aq, existed in de-ashed biochars. Although hydrozincite is Zn mineral, the formation of small amounts of hydrozincite in de-ashed biochars may be caused by the dissolution of CO_2 in the air. The pH_{PZC} of de-ashed biochars were 4.3–5.5 (Table 1), thus when the solution pHs were controlled to 7, the de-ashed biochars could easily adsorb few amount of Zn^{2+}.

The Ions Involved in Zn Immobilization. According to the analysis of XRD and EXAFS, we have identified the main Zn species formed on biochars. To examine these results, the pHs of the samples withdrawn at 2 h and the concentrations of CO_3^{2-} and Si species in the samples withdrawn at 120 h in kinetics experiments were determined. For comparison, these determinations were also conducted on their corresponding blank samples (0.1 g of biochar + 25 mL of water). The concentrations of PO_4^{3-}, Ca^{2+}, and Mg^{2+} were also determined. The samples in kinetics experiments are denoted as B + Zn, and the blank samples are denoted as B.

As shown in Table 2, the pHs of B + Zn at the reaction time of 2 h reached 7.0, which were lower than those of B. This indicated that plenty of OH^- were consumed during Zn immobilization. For PN350 and WS350, the concentrations of CO_3^{2-} in B were respectively 0.3 and 1.1 mmol L^{-1}; while the concentrations of CO_3^{2-} in B + Zn could not be detected (ND) indicating the consumption of CO_3^{2-} during Zn immobilization. As Ca^{2+} which released from biochars could also react with CO_3^{2-}, the amount of CO_3^{2-} which would react with Zn to form hydrozincite would be underestimated from these results. The released Si species could also influence the determination of CO_3^{2-}, as they could buffer H^+ in the solution[44], which lead to the overestimated concentrations of CO_3^{2-}. Thus the concentrations of CO_3^{2-} in different samples cannot be used to calculate the real amounts of consumed CO_3^{2-} in Zn immobilization, they were only for reference. For WS350 and WS550, the Si concentrations in B were respectively 0.9 and 2.0 mmol L^{-1} (the initial concentration of Zn^{2+} was 2.3 mmol L^{-1}). Once reacted with Zn^{2+}, the concentrations of Si decreased drastically. From the considerable amounts of released and consumed Si species, we assumed that some Si species in WS biochars may play an important role in Zn immobilization. Fig. S6 shows the ATR-FTIR spectra of the raw biochar filtrates. From Figs S6a and S6b we cannot see any band present in the spectra, while in Figs S6c and S6d there is a broad band in the region 1150–1050 cm^{-1} in each of the spectrum, which is due to the asymmetric Si–O–Si stretching vibration of long chain polymers[45]. The ATR-FTIR result suggested that the Si species released from biochar are Si-containing polymers with different chain length. The release and consumption of OH^-, CO_3^{2-} and Si species confirmed the results of XRD and EXAFS.

The difference on the concentrations of PO_4^{3-} between B and B + Zn implied the formation of $Zn_3(PO_4)_2$ on biochars, however the concentrations of PO_4^{3-} in B were no more than 0.06 mmol L^{-1}, thus the precipitation role of PO_4^{3-} in the studied biochars can be ignored. The concentrations of Ca^{2+} and Mg^{2+} in B + Zn were much higher than those of Ca^{2+} in B; expect for the condition of PN350, the concentrations of Mg^{2+} in B + Zn were also higher than those of Mg^{2+} in B. This may be caused by the competition of Zn^{2+} for released OH^-, CO_3^{2-}, and some sorption sites. When raw biochar was added into water, plenty of ions such as Ca^{2+}, Mg^{2+}, OH^-, and CO_3^{2-} were released from biochar to bulk solution. With the gradual increase in concentrations of Ca^{2+}, Mg^{2+}, and anions such as OH^-, CO_3^{2-} in the solution close to biochar surface, some of these ions would be over-saturated, Ca, Mg-precipitates would form and deposit on the surface of biochar. In addition to forming precipitates, a portion of Ca^{2+} and Mg^{2+} could also be captured by oxygen-containing functional groups of biochar. Thus, in

raw biochar-water systems, the newly released Ca^{2+} and Mg^{2+} can be immobilized rapidly. When Zn^{2+} was present in the solution, Zn^{2+} would diffuse to the area close to biochar surface, they could also react with the newly released anions (i.e. OH^- and CO_3^{2-}) and occupy the sorption sites (i.e. oxygen-containing functional groups of biochar). This process would decrease the concentrations of OH^-, CO_3^{2-}, and PO_4^{3-} and sorption sites of Ca^{2+} and Mg^{2+}, which further resulted in the increased amounts of released Ca^{2+} and Mg^{2+} in raw biochar-Zn solution systems (B + Zn). The low sorption capacity of Zn^{2+} on PN350 and inhomogeneous distribution of Mg on biochar may lead to the lower concentration of Mg^{2+} in B(PN350) + Zn, when compared with those of Mg^{2+} in B(PN350) + Zn.

The Possible Evolution Processes of OH^-, CO_3^{2-}, and Si Species on Biochars. To reveal the immobilization mechanism of Zn on biochars, we first need to know the formation rule of OH^-, CO_3^{2-}, and Si Species. Although few studies can describe the clear evolution processes of ash in biochar, we may obtain the general evolution processes based on the pyrolysis rule of biomass.

In plants, some alkali and alkaline earth metal (AAEM), e.g. K, Ca, and Mg, are associated with organic molecules[46]. During pyrolysis, with the decomposition of the organic matters and reconstruction of the remaining parts, biomass transformed into char (not the ultimate biochar), and AAEMs were then bonded to the char in the form of C–O–Met^+ or C–O–Met^{2+}–O–C (Met^+ represents K^+, and Met^{2+} represents Ca^{2+} and Mg^{2+})[47]. Once the bonds between AAEMs and char were attacked by free radicals which were formed in pyrolysis, elemental AAEMs were formed[47–50]. As these species are not stable, they would be easily oxidized to form metal oxides and react with H_2O, which was released from biomass during pyrolysis, to form AAEM hydroxides (see Equation 1, M represents elemental AAEMs, such as K, Ca, or Mg). These AAEM hydroxides could be the source of released OH^- in the solution. The decomposition of cellulose and lignin[18,51] lead to the generation of CO_2. CO_2 may react with H_2O and newly formed AAEM hydroxides to form various carbonates (see Equations 2 and 3). Thus, in addition to the carbonates contained in the raw biomass, the newly formed carbonates during pyrolysis could also be the source of CO_3^{2-} in the solution. The Si species are much more stable than other inorganic species in biomass[18,52]. It is reported that the main forms of Si in wheat biomass are amorphous silica and silicate esters[53,54], the forms of these Si species would change when the water in biomass evaporated and the organic matters decomposed during pyrolysis, some of the Si species would transform into quartz (see Fig. 2) and dehydroxylated silicates[18], some of them would transformed into alkali silicates (such as K_2SiO_3)[52]. Without the protection of organic matters, the exposed Si species can be easily released to the solution. Among the Si species formed on biochar, alkali silicates are soluble compounds, the solutions of which contain a wide variety of polysilicate ions[55] (consist with the ATR-FTIR results of raw biochar filtrates). Thus alkali silicates are probably the Si species released into water or Zn solution.

$$M_2O_x + xH_2O \rightarrow 2M(OH)_x \quad (1)$$

$$CO_2 + H_2O \rightarrow H_2CO_3 \quad (2)$$

$$xH_2CO_3 + 2M(OH)_x \rightarrow 2xH_2O + M_2(CO_3)_x \quad (3)$$

From the proposed evolution processes of the anions, we find that the formation of these ions are closely related to the decomposition of biomass, and the higher degree of decomposition (higher pyrolysis temperature) will lead to the higher amounts of OH^-, CO_3^{2-}, and Si species presented on biochar surface. Some previous studies have also found this phenomenon. Yuan *et al.* reported that the pHs and carbonate contents of biochar derived from different straws increased with pyrolysis temperature[56]; Xiao *et al.* found that the dissolved Si species released from biochar prepared by rice straw increased[33] when the temperature increased from 250 °C to 700 °C.

The Immobilization Mechanism of Zn on PN and WS Biochars. The formation of various ashes on biochars is the premise for Zn immobilization; and the formation of different Zn species is the immobilization mechanism of Zn on PN and WS biochars. The formation processes of the main Zn species (the fractions of which are higher than 10%) on different biochars are proposed and described as follows (Fig. 4).

For PN350 and WS350, once biochars were added into Zn solution, the OH^- and CO_3^{2-}, which were formed on biochar during pyrolysis[56], tend to release into bulk solution. As OH^- and CO_3^{2-} were released from biochar, at the early stage of the diffusion the concentrations of OH^- and CO_3^{2-} in the solution close to biochar surface were much higher than those of bulk solution. Under this condition, when Zn^{2+} diffused to biochar surface, these ions were easily over-saturated and form hydrozincite and $Zn(OH)_2$ (Fig. 4, Paths 1 and 2), and finally deposited on biochar surface. For biochars produced at low temperature (i.e. 350 °C), there existed a large portion of oxygen-containing functional groups (i.e. carboxyl and hydroxyl)[24]. When they presented in the solution with high pH, these functional groups will be deprotonated and adsorb Zn^{2+}. During the process of Zn immobilization, the solution pHs were not controlled, they decreased from >9 to 7 with reaction time. From the calculation of Visual MINTEQ 3.1 (Supplementary Fig. S7), we find that two Zn species (i.e. Zn^{2+} and $Zn(OH)^+$) could be involved in the reaction, and the proportion of Zn^{2+} was much higher than that of $Zn(OH)^+$. The reactions were shown in Fig. 4, Path 3. Although the sorption mechanisms of PN350 and WS350 are the same, the sorption capacity of Zn on PN350 are much lower than that on WS350, which may be due to the lower amounts of OH^-, CO_3^{2-} and oxygen-containing functional groups formed on PN350 when compared with those formed on WS350. This phenomenon implied that different feedstocks have different degree of decomposition under the same pyrolysis temperature, which would lead to different sorption performances of biochars.

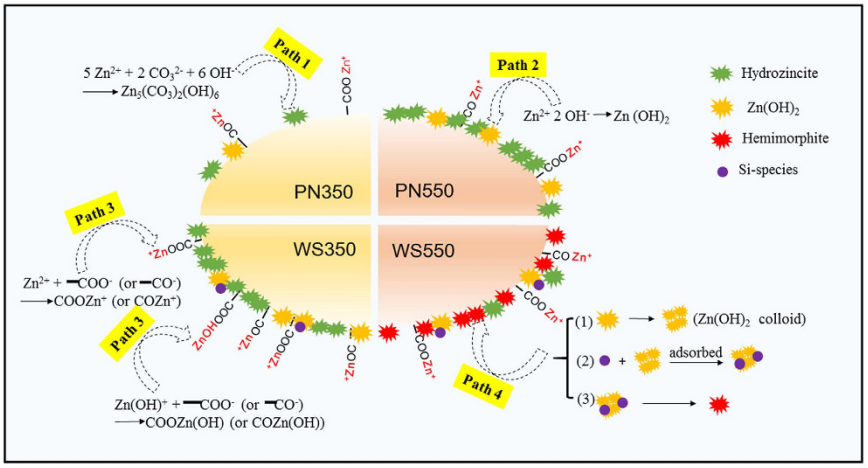

Figure 4. The formation process of the main Zn species on different biochars.

For PN550 and WS550, with the volatilization of organic matters and completion of thermal decompositions, the ash content increased, which made the fraction of Zn precipitates/minerals close to 100%. Compared with PN350, PN550 contained much more CO_3^{2-} and OH^-, thus the sorption capacity of Zn on PN550 was higher than that of PN350. For WS550, a large fraction of hemimorphite was formed. This was due to a considerable amount of released Si species. The formation of hemimorphite on WS550 can be divided into three steps[57] (Fig. 4, Path 4): (1) the formation of colloid of $Zn(OH)_2$ under alkaline condition, (2) the adsorption of dissolved silicates on $Zn(OH)_2$ colloid and co-precipitation of silicate and $Zn(OH)_2$, and (3) the reconstruction of the co-precipitates structure and formation of amorphous hemimorphite. Due to the complexity of the sorption system and short reaction time, the well-crystallized hemimorphite was unlikely to form. Thus, it cannot be detected by the method of XRD. Although there were also some Si species released from WS350, only a small portion of hemimorphite was formed. This may be caused by the low amounts of OH^- and Si species released from WS350 biochar.

The formation of different Zn species on biochars confirmed heterogeneous property of these materials which resulted in the co-existence of various sorption mechanisms during Zn retention by biochars. The consumption of OH^-, CO_3^{2-}, or the sorption sites (oxygen-containing functional groups) on biochars by Zn^{2+} to form different Zn species led to the release of Ca^{2+} and Mg^{2+}. When the studied raw biochars were added into the acid solutions, the ions OH^- and CO_3^{2-} in biochar were consumed and even some oxygen-containing functional groups were protonated. This was against the formation of different Zn species, which could lead to the decrease in the sorption capacities of Zn on biochars.

Conclusion

The ash in PN and WS biochars played important role on Zn immobilization. The higher pyrolysis temperature on the feedstock leads to the higher sorption capacity of Zn^{2+} and the larger fraction of Zn precipitates/minerals on biochar. Hydrozincite and $Zn(OH)_2$ were the main species formed on PN350, PN550, and WS350; while on WS550, besides hydrozincite, a large fraction of hemimorphite was formed. The formation of OH^-, CO_3^{2-}, and Si species on biochars and the release of these species played predominant role on Zn immobilization.

Materials and Methods

Preparation of Raw Biochars and De-ashed Biochars. Biochars derived from PN and WS were prepared in a patented biochar reactor (NO. ZL2009 2 0232191.9) under oxygen-limited conditions. According to the decomposition rule of the feedstocks obtained from thermal analysis, 350 °C and 550 °C were selected as the pyrolysis temperatures (See Supplementary S2). To remove the ash on biochars, HCl/HF (1.0 M, v/v 1:1) solution was used to wash the raw biochars for several times. The details for biochar preparation were shown in Supplementary S2. The biochar sample derived from PN (WS) at 350 °C and 550 °C were denoted as PN350 (WS350) and PN550 (WS550), respectively. The de-ashed biochar were denoted as $PN350_D$, $PN550_D$, $WS350_D$, and $WS550_D$.

Sorption Kinetics and Sorption Isotherms. One hundred milligram of raw biochars or de-ashed biochars were added into 25 mL of $Zn(NO_3)_2$ solutions in 50 mL vials. These vials were shaken at 200 rpm at 25 °C. For raw biochars, the Zn^{2+} concentration in $Zn(NO_3)_2$ solution was 150 mg L^{-1} and the pH of the solution was not adjusted. For the sorption experiments of de-ashed biochars, the Zn^{2+} concentration was 50 mg L^{-1} and the pH of the solution was adjusted to 7 buffered by 5 mM MOPs. The samples were withdrawn at appropriate time intervals, then the mixture was filtered with a 0.45 μm membrane, and the Zn^{2+} concentrations of the filtrates were determined. The sorption capacity of biochar in each time interval was obtained by Supplementary Equation S1. The concentrations of CO_3^{2-}, Si species, PO_4^{3-}, Ca^{2+}, and Mg^{2+} were also determined in the samples withdrawn at 120 h, then concentrations of these five species in the filtrates of blank samples (0.1 g of biochar + 25 mL of water) at 120 h were determined for comparison. The concentrations of Zn^{2+}, Ca^{2+} and Mg^{2+} were determined using Atomic Absorption Spectrometer (AAS, Hitachi-Z2000, High-Technologies Corporation,

Japan); the concentrations of CO_3^{2-} were determined using titration method[44]; the concentrations of Si species were determined using Inductively Coupled Plasma – Atomic Emission Spectrometer (ICP-AES, OPTIMA 8000, PerkinElmer, USA); and the concentrations of PO_4^{3-} were determined using molybdate-ascorbic acid method. Two parallel samples were applied in sorption samples. Sorption isotherms were performed the same way as sorption kinetics except for the initial concentrations of Zn^{2+} applied (see Supplementary S6).

Effect of Initial pH. Fifty milligram of raw biochars or de-ashed biochars were added into 23 mL of deionized (DI) water in 50 mL vials. These vials were shaken at 200 rpm at 25 C for 3 day equilibrium. Then the pHs of the mixtures in these vials were adjusted to 2–10. Certain amount of $Zn(NO_3)_2$ stock solution was dripped into each vial to make the initial concentration of Zn^{2+} to be 150 mg L^{-1} for raw biochar and 50 mg L^{-1} for de-ashed biochar. DI water was then added into the vial to make the solution volume up to 25 mL. The following procedure was the same as that of isotherms experiments and the sorption capacity of biochar was obtained by Supplementary Equation S6.

Characterization of Feedstocks and Biochars. The thermal properties of PN and WS were obtained using a Thermogravimertic Analyzer (TGA, Pyris 1 TGA, PerkinElmer, USA) at 20 °C/min up to the final temperature of 700 °C under a flow of N_2. The functional groups of biochar and the Si species in the filtrates of raw biochar were analyzed using Fourier Transform Infrared Spectroscopy (FTIR, Nicolet FTIR IS10, Thermo Scientific, USA). The methods of sample preparation and data analysis are shown in Supplementary S8. The surface of biochar was analyzed with X-ray Photoelectron Spectrometer (XPS, PHI-5000 Versaprobe, ULVAC-PHI, Japan) using an Al Kα excitation radiation. The pHs of raw biochars and pHs of point of zero charge (pH_{PZC}) of de-ashed biochars were obtained by the pH drift method in Supplementary S9 and S10. The contents of K, Ca, Mg, Al, Fe, Zn, and P in biochars were analyzed after the microwave digestion of biochars with HNO_3-HF-H_2O_2 (U.S. EPA 3502)[58]. The concentrations of K, Al, and Fe in the digestion solution were determined with ICP-AES. The digestion experiments were conducted in duplicate for each biochar.

Characterization of Zn Species on Biochars. The minerals in biochars were analyzed by X-ray Powder Diffraction (XRD). The tests were performed on a Rigaku, Ultima IV Diffractmeter (Rigaku Corporation, Japan), and Cu Kα radiation generated at 40 kV/40 mA, data were collected in the range (2θ) from 0° to 60° with the scan step of 0.02°. The minerals in the samples were identified using the XRD data analysis software (MDI JADE 6.5) and its corresponding powder diffraction file (PDF) database. The Zn species on biochars were analyzed by the method of extended X-ray Absorption Fine Structure (EXAFS) spectroscopy in fluorescence modes. Zn K-edge (9659 eV) measurements were carried out at beamline BL14W at the Shanghai Synchrotron Radiation Facility Center (SSRF). Principal Component Analysis (PCA) accompanied with Linear Combination Fitting (LCF) were used for species identification and quantification. The details of EXAFS spectra collection and data processing were shown in Supplementary S11.

References

1. Ebbs, S. D. & Kochian, L. V. Toxicity of zinc and copper to Brassica species: Implications for phytoremediation. *J. Environ. Qual.* **26,** 776–781 (1997).
2. Tkalec, M. *et al.* The effects of cadmium-zinc interactions on biochemical responses in tobacco seedlings and adult plants. *Plos one* **9,** e87582 (2014).
3. Chaney, R. Zinc phytotoxicity. In *Zinc in soils and plants* (ed. Robson, A. D.) 135–150 (Perth, 1993).
4. Beyer, W., Green, C., Beyer, M. & Chaney, R. Phytotoxicity of zinc and manganese to seedlings grown in soil contaminated by zinc smelting. *Environ. Pollut.* **179,** 167–176 (2013).
5. Maderova, L. & Paton, G. I. Deployment of microbial sensors to assess zinc bioavailability and toxicity in soils. *Soil Biol. Biochem.* **66,** 222–228 (2013).
6. Macdonald, C. A. *et al.* Relative impact of soil, metal source and metal concentration on bacterial community structure and community tolerance. *Soil Biol. Biochem.* **42,** 1408–1417 (2010).
7. Khellaf, N. & Zerdaoui, M. Phytoaccumulation of zinc by the aquatic plant, Lemna gibba L. *Bioresour. Technol.* **100,** 6137–6140 (2009).
8. Lin, W. *et al.* Hyperaccumulation of zinc by Corydalis davidii in Zn-polluted soils. *Chemosphere* **86,** 837–842 (2012).
9. Barone, A., Ebesh, O., Harper, R. G. & Wapnir, R. A. Placental copper transport in rats: effects of elevated dietary zinc on fetal copper, iron and metallothionein. *J. nutr.* **128,** 1037–1041 (1998).
10. Gyorffy, E. J. & Chan, H. Copper deficiency and microcytic anemia resulting from prolonged ingestion of over–the–counter zinc. *Am. J. Gastroenterol.* **87** (1992).
11. Nguyen, B. T. *et al.* Long-term black carbon dynamics in cultivated soil. *Biogeochemistry* **92,** 163–176 (2009).
12. Atkinson, C. J., Fitzgerald, J. D. & Hipps, N. A. Potential mechanisms for achieving agricultural benefits from biochar application to temperate soils: a review. *Plant Soil* **337,** 1–18 (2010).
13. Cao, X. D., Ma, L. N., Liang, Y., Gao, B. & Harris, W., Simultaneous Immobilization of Lead and Atrazine in Contaminated Soils Using Dairy-Manure Biochar. *Environ. Sci. Technol.* **45,** 4884–4889 (2011).
14. Huang, J. H., Hsu, S. H. & Wang, S. L. Effects of rice straw ash amendment on Cu solubility and distribution in flooded rice paddy soils. *J. Hazard. Mater.* **186,** 1801–1807 (2011).
15. Keith, A., Singh, B. & Singh, B. P. Interactive Priming of Biochar and Labile Organic Matter Mineralization in a Smectite-Rich Soil. *Environ. Sci. Technol.* **45,** 9611–9618 (2011).
16. Uchimiya, M., Wartelle, L. H. & Boddu, V. M. Sorption of Triazine and Organophosphorus Pesticides on Soil and Biochar. *J. Agr. Food Chem.* **60,** 2989–2997 (2012).
17. Ahmad, M. *et al.* Biochar as a sorbent for contaminant management in soil and water: A review. *Chemosphere* **99,** 19–33 (2014).
18. James, A. & Stephen, J. Characteristics of biochar: Microchemical properties. In *Biochar for Environmental Management: Science and Technology* (ed. Lehmann, J. & Joseph, S.) 33–49 (London, 2009).
19. Cheng, C. H. *et al.* Oxidation of black carbon by biotic and abiotic processes. *Org. Geochem.* **37,** 1477–1488 (2006).
20. Chen, B., Zhou, D. & Zhu, L. Transitional adsorption and partition of nonpolar and polar aromatic contaminants by biochars of pine needles with different pyrolytic temperatures. *Environ. Sci. Technol.* **42,** 5137–5143 (2008).
21. Chen, Z., Chen, B., Zhou, D. & Chen, W. Bisolute sorption and thermodynamic behavior of organic pollutants to biomass-derived biochars at two pyrolytic temperatures. *Environ. Sci. Technol.* **46,** 12476–12483 (2012).

22. Hale, S. *et al.* Effects of chemical, biological, and physical aging as well as soil addition on the sorption of pyrene to activated carbon and biochar. *Environ. Sci. Technol.* **45,** 10445–10453 (2011).
23. Liu, X. Q. *et al.* Pyrolytic temperature dependent and ash catalyzed formation of sludge char with ultra-high adsorption to 1-naphthol. *Environ. Sci. Technol.* **50,** 2602–2609 (2016).
24. Chan, K. Y. & Xu, Z. H. Biochar: Nutrient properties and their enhancement. In *Biochar for Environmental Management: Science and Technology* (ed. Lehmann, J. & Joseph, S.) 67–81 (London, 2009).
25. Pan, J. J., Jiang, J. & Xu, R. K. Adsorption of Cr(III) from acidic solutions by crop straw derived biochars. *J. Environ. Sci.-China* **25,** 1957–1965 (2013).
26. Beesley, L. & Marmiroli, M. The immobilisation and retention of soluble arsenic, cadmium and zinc by biochar. *Environ. Pollut.* **159,** 474–480 (2011).
27. Melo, L. C. *et al.* Sorption and desorption of cadmium and zinc in two tropical soils amended with sugarcane-straw-derived biochar. *J. Soil. Sediment.* **16,** 226–234 (2016).
28. Xu, X. *et al.* Removal of Cu, Zn, and Cd from aqueous solutions by the dairy manure-derived biochar. *Environ. Sci. Pollut. R.* **20,** 358–368 (2013).
29. Betts, A. R., Chen, N., Hamilton, J. G. & Peak, D. Rates and mechanisms of Zn^{2+} adsorption on a meat and bonemeal biochar. *Environ. Sci. Technol.* **47,** 14350–14357 (2013).
30. Wagner, A. *et al. Biochar-induced formation of Zn–P-phases in former sewage field soils studied by PK-edge XANES spectroscopy*. **178,** 582–585 (2015).
31. Mukherjee, A., Zimmerman, A. R. & Harris, W. Surface chemistry variations among a series of laboratory-produced biochars. *Geoderma* **163,** 247–255 (2011).
32. Budai, A. *et al.* Surface Properties and Chemical Composition of Corncob and Miscanthus Biochars: Effects of Production Temperature and Method. *J. Agr. Food Chem.* **62,** 3791–3799 (2014).
33. Xiao, X. *et al.* Transformation, morphology, and dissolution of silicon and carbon in rice straw-derived biochars under different pyrolytic temperatures. *Environ. Sci. Technol.* **48,** 3411–3419 (2014).
34. Lee, J. W. *et al.* Characterization of biochars produced from cornstovers for soil amendment. *Environ. Sci. Technol.* **44,** 7970–7974 (2010).
35. Ho, Y. S. & McKay, G. Pseudo-second order model for sorption processes. *Process Biochem.* **34,** 451–465 (1999).
36. Chien, S. H. & Clayton, W. R. Application of elovich equation to the kinetics of phosphate release and sorption in soils. *Soil Sci. Soc. Am. J.* **44,** 265–268 (1980).
37. Zhou, Y. T. *et al.* Adsorption mechanism of Cu^{2+} from aqueous solution by chitosan-coated magnetic nanoparticles modified with α-ketoglutaric acid. *Colloid. Surface. B.* **74,** 244–252 (2009).
38. Tütem, E., Apak, R. & Ünal, Ç. F. Adsorptive removal of chlorophenols from water by bituminous shale. *Water Res.* **32,** 2315–2324 (1998).
39. Weber, W. J. & Morris, J. C. Kinetics of adsorption on carbon from solution. *Journal of the Sanitary Engineering Division* **89,** 31–60 (1963).
40. Foo, K. Y. & Hameed, B. H. Insights into the modeling of adsorption isotherm systems. *Chem. Eng. J.* **156,** 2–10 (2010).
41. Sarret, G. *et al.* Zn speciation in the organic horizon of a contaminated soil by micro-X-ray fluorescence, micro- and powder-EXAFS spectroscopy, and isotopic dilution. *Environ. Sci. Technol.* **38,** 2792–2801 (2004).
42. Isaure, M. P. *et al.* Quantitative Zn speciation in a contaminated dredged sediment by μ-PIXE, μ-SXRF, EXAFS spectroscopy and principal component analysis. *Geochim. Cosmochim. Ac.* **66,** 1549–1567 (2002).
43. Scheinost, A. C., Kretzschmar, R., Pfister, S. & Roberts, D. R. Combining selective sequential extractions, X-ray absorption spectroscopy, and principal component analysis for quantitative zinc speciation in soil. *Environ. Sci. Technol.* **36,** 5021–5028 (2002).
44. Pansu, M. & Gautheyrou, J. *Handbook of Soil Analysis: Mineralogical, Organic and Inorganic Methods* (ed. Pansu, M. & Gautheyrou, J.) 616–617 (Berlin, 2006).
45. Socrates, G. Organic silicon compounds In *Infrared and Raman characteristic group frequencies: tables and charts*. (ed. Socrates, G.) 246–247 (New York, 2001).
46. Hawkesford, M. *et al.* Functions of Macronutrients In *Marschner's mineral nutrition of higher plants*. (ed. Marschner, H.) 165–172 (San Diego, 2012).
47. Sonoyama, N. *et al.* Interparticle Desorption and Re-adsorption of Alkali and Alkaline Earth Metallic Species within a Bed of Pyrolyzing Char from Pulverized Woody Biomass. *Energ. Fuel.* **20,** 1294–1297 (2006).
48. Keown, D. M., Favas, G., Hayashi, J. i. & Li, C. Z. Volatilisation of alkali and alkaline earth metallic species during the pyrolysis of biomass: differences between sugar cane bagasse and cane trash. *Bioresour. Technol.* **96,** 1570–1577 (2005).
49. Quyn, D. M., Wu, H. & Li, C. Z. Volatilisation and catalytic effects of alkali and alkaline earth metallic species during the pyrolysis and gasification of Victorian brown coal. Part I. Volatilisation of Na and Cl from a set of NaCl-loaded samples. *Fuel* **81,** 143–149 (2002).
50. Li, C. Z., Sathe, C., Kershaw, J. & Pang, Y. Fates and roles of alkali and alkaline earth metals during the pyrolysis of a Victorian brown coal. *Fuel* **79,** 427–438 (2000).
51. Liu, Q. *et al.* Mechanism study of wood lignin pyrolysis by using TG–FTIR analysis. *J. Anal. Appl. Pyrol.* **82,** 170–177 (2008).
52. Okuno, T. *et al.* Primary release of alkali and alkaline earth metallic species during the pyrolysis of pulverized biomass. *Energ. Fuel.* **19,** 2164–2171 (2005).
53. Jarvis, S. C. The uptake and transport of silicon by perennial ryegrass and wheat. *Plant Soil* **97,** 429–437 (1987).
54. Broadley, M. *et al.* Beneficial elements In *Marschner's mineral nutrition of higher plants*. (ed. Marschner, H.) 257–258 (San Diego, 2012).
55. Miniham, A. Silicates. In *Ullmann's encyclopedia of industrial chemistry* (ed. Wiley-VCH Verlag GmbH & Co.) 55–56 (Weinheim, 2005).
56. Yuan, J. H. *et al.* The forms of alkalis in the biochar produced from crop residues at different temperatures. *Bioresour. Technol.* **102,** 3488–3497 (2011).
57. Nagata, H., Matsunaga, M. & Hosokawa, K. Analytical study of the formation process of hemimorphite-part I analysis of the crystallization process by the co-precipitation method. *Zairyo-to-Kankyo* **42,** 225–233 (1999).
58. United States Environmental Protection Agency (U.S. EPA). Microwave assisted acid digestion of siliceous and organically based matrics. In Test Methods for Evaluating Solid Waste, Method 3052; U.S. EPA: Washington, D.C. 1996.

Acknowledgements

This research was supported by the National Science Foundation for Young Scientists of China (41501247), the National Natural Science Foundation of China (41422105, 21537002, 41401252), the Natural Science Foundation of Jiangsu Province of China (BK20141047), and Jiangsu Planned Projects for Postdoctoral Research Funds (1402117C). We would like to thank the Shanghai Synchrotron Radiation Facility for use of the synchrotron facilities at beamline BL14W.

Author Contributions

T.Q. conceived and carried out most of the experiments, analyzed the data, and wrote the manuscript; Y.W. and T.Q. analyzed the EXAFS data; T.F. conducted the EXAFS experiments; D.Z. supervised this work; D.Z. and G.F. edited this manuscript and provided important advices. All authors discussed the results and contributed to the manuscript.

Additional Information

Supplementary information accompanies this paper at http://www.nature.com/srep

Competing financial interests: The authors declare no competing financial interests.

How to cite this article: Qian, T. *et al.* A new insight into the immobilization mechanism of Zn on biochar: the role of anions dissolved from ash. *Sci. Rep.* **6**, 33630; doi: 10.1038/srep33630 (2016).